Placement and sizing of solar PV and Wind systems in trolleybus grids

Diab, Ibrahim; Scheurwater, Bram ; Saffirio, Alice ; Chandra-Mouli, Gautham Ram; Bauer, Pavol

DOI
10.1016/j.jclepro.2022.131533

Publication date
2022

Document Version
Final published version

Published in
Journal of Cleaner Production

Journal of Cleaner Production 352 (2022) 131533

Contents lists available at ScienceDirect

Journal of Cleaner Production

journal homepage: www.elsevier.com/locate/jclepro

Placement and sizing of solar PV and Wind systems in trolleybus grids ☆

Ibrahim Diab *, Bram Scheurwater, Alice Saffirio, Gautham Ram Chandra-Mouli, Pavol Bauer

Technische Universiteit Delft (TU Delft), Faculty of Electrical Engineering, Mathematics, and Computer Science, Electrical Sustainable Energy Department, Mekelweg 4, 2628 CD Delft, The Netherlands

ARTICLE INFO

Handling Editor: Zhifu Mi

Keywords:
DC systems
Electric mobility
Public transport
Solar PV
Trolleybus
Wind energy

ABSTRACT

Reducing the environmental impact of transportation requires the successful integration of renewable energy sources into the electrical transportation networks. However, the mismatch between renewable generation and the intermittent bus schedules causes temporary absence of loads and creates considerable excess energy, potentially rendering the systems economically infeasible. So far, studies on integration of renewables in transport grids were limited to decentralized solar PV systems (placed at the substation level), using statistical or simplified models, and concerned mainly with increasing the trolleygrid capacity. In this paper, both PV and Wind systems are considered and studied as to maximize their direct utilization by using verified simulation models for six different sizing and placement scenarios. The Dutch trolleygrid of Arnhem is used as a case study. Scenarios I to V looked at a decentralized renewable sources placement and ultimately concluded that PV systems at low-traffic substations are best sized for complete energy-neutrality, with daily storage systems. On the other hand, those at high-traffic substations should be without storage and sized below their energy-neutrality point — ideally, using the Marginal Utilization approach (scenario III). Finally, the Centralized (Aggregated) Energy-Neutral Wind and PV Approach of scenario VI offers the best outcome, with a hybrid solution of 53% PV and 47% Wind. This scenario offers a 54.1% direct bus load coverage. In comparison, scenario I, which had attempted a grid energy-neutrality in a decentralized manner, had only achieved 32.4% direct load coverage. The outcome of scenario VI can even be pushed to values above 80% by installing storage systems.

1. Introduction

Transport accounts for about 24% of the world CO2 emissions, making transportation electrification a necessary step toward sustainability (Europea, 2013; Wang et al., 2007). Fortunately, the electrification of urban public transport is already growing in momentum, and current trends predict by 2030 a market penetration of up to 75% (Alliance, 2019). This, however, is counter-productive if the transportation system is still fed with electricity coming from fossil fuels.

In particular, recent advancements in battery technologies and electric mobility have allowed transportation players such as trolleybuses to re-enter the urban transport landscape (Fitzová and Matulová, 2020; Kołoś and Taczanowski, 2016; Borowik and Cywiński, 2016). Trolleybuses are destined to become a key player in this field, after decades of expansion and contraction that saw many of their networks going out of commission (Wołek et al., 2021; Brunton, 1992). Their electrical grids are becoming increasingly more sophisticated with the inclusion of smart grid technologies (Bartłomiejczyk, 2018b). In fact, DC trolleygrids are ushering in a new era of active, urban transportation grids as they look at integrating solar PV (Bartłomiejczyk, 2018a; Kratz et al., 2019, 2018; Salih et al., 2018a,b; Wazifehdust et al., 2019), on-board and/or off-board storage (Rufer et al., 2004; Zhang et al., 2015; Iannuzzi et al., 2012; Zhang et al., 2017), electric-vehicle (EV) chargers (Shekhar et al., 2021; Salih et al., 2018a; Wu et al., 2020), and In-Motion-Charging (IMC) buses (Bartłomiejczyk, 2017; Wołek et al., 2021) into their network.

1.1. The trolleybus grid

A trolleybus is a bus that operates by DC overhead cables (Fig. 1). A substation that consists of a step-down transformer and a rectifier turns the Low Voltage AC (LVAC) to a low voltage DC at about 650–750 V. The substations connect to its sections via feeder cables. When the buses are braking, their regenerative-braking energy can be shared with buses on the same section. They can also send this power to a bus on a connected section under the same substation. Bus1 and Bus2 in Fig. 1, for example, can share power via the path feedercable1-substation

☆ This document is the results of the research project funded by Trolley2.0.
* Corresponding author.
E-mail address: i.diab@tudelft.nl (I. Diab).

https://doi.org/10.1016/j.jclepro.2022.131533
Received 8 November 2021; Received in revised form 20 March 2022; Accepted 23 March 2022
Available online 1 April 2022

Abbreviations

EV	Electric Vehicles
HVAC	Heating, Ventilation, and Air Conditioning
IMC	In-Motion-Charging
LVAC	Low Voltage AC
RES	Renewable Energy Sources
SS	Substation
STC	Standard Testing Conditions

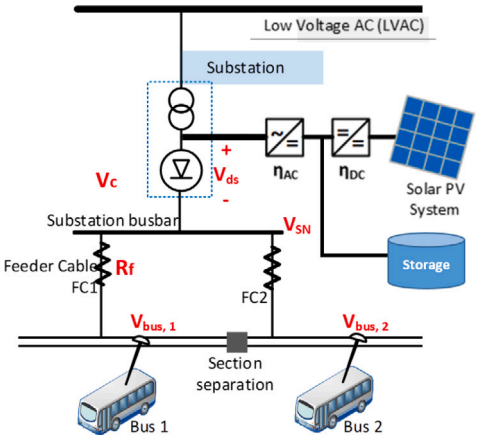

Fig. 1. The trolleygrid and its components with the solar PV system installed on the AC side.

busbar-feedercable2. The braking power cannot be sent back to the AC grid because the substation rectifiers make the system unidirectional. Therefore, in the absence of another receiving bus in the vicinity, the braking energy is wasted in on-board braking resistors. Some new works are investigating bidirectional substations that can send power back to the AC grid, but are beyond the scope of this paper (Cornic, 2010; Warin et al., 2011).

The vision of the trolleygrid of the future is an active, multi-functional grid with integrated Renewable Energy Sources (RES) such as solar PV or Wind, energy storage systems, and Electric Vehicles (EV) chargers. In-Motion-Charging (IMC) buses, a hybrid between trolley- and e-buses, are also players in this future grid. Integrating RES into the grid could alleviate a part of the energy demand from the AC grid and increase the capacity of the future DC trolleygrid. PV systems, for example, are DC, scalable, and urban-friendly. This makes them an attractive solution for the sustainable powering of urban transport networks. However, one main challenge is that the trolleybuses, like any transportation system, run on a schedule with some time interval in between vehicles. This results in sections of the grid experiencing long periods of zero bus demand while the PV system is generating power as seen in the simulations of Fig. 2 of the dutch city of Arnhem. Moreover, the PV system does not generate power at night, while the buses are still operational.

This calls for a storage system, an exchange with the AC grid for later-use (storing in the grid), or even curtailing (wasting) the excess generation. These modes are explained in Fig. 3. Moreover, the PV generation peaks in the summer while the trolleygrid is at its lowest demand requirements. This is because in the summer, the buses run on lower-traffic schedules and without the significant bus load of Heating, Ventilation, and Air Conditioning (HVAC) which constitutes half of the demand of the winter months (Tomar et al., 2018).

This mismatch has also made wind energy an attractive RES option. Fig. 4 shows that the wind generation as a trend matches the trolleybus demand better than the PV on a yearly scale. Additionally, wind power

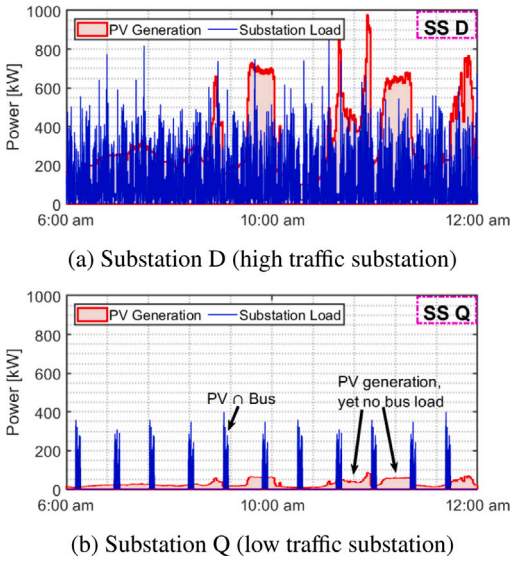

(a) Substation D (high traffic substation)

(b) Substation Q (low traffic substation)

Fig. 2. Mismatch in simulated PV generation and the bus load for two Arnhem substations. The simulation methodology is detailed in Section 2.

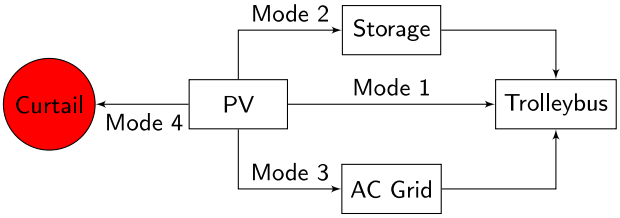

Fig. 3. The PV power flow: Generated energy can be used directly by the trolleybus (mode 1, most desirable), kept in the storage for later use by the trolleybus (mode2), sent to the AC Grid – if local policy allows it – to be used later by the trolleybus (mode 3, net metering), or curtailed (mode 4, wasted).

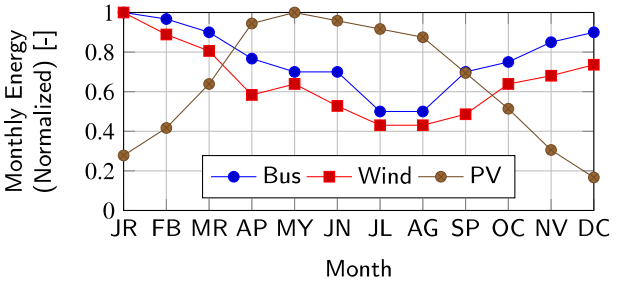

Fig. 4. Yearly simulated bus demand, wind generation, and PV generation trends by month for the entire Arnhem grid. Each variable is normalized with respect to the highest monthly value it reports. It is observable that the wind generation better follows the bus demand trend on a yearly basis.

is available after sunset, so it can cover the demand of night buses. However, the simulations of the whole trolleygrid of Arnhem in Fig. 5, show that the PV is still an interesting option as it better matches the bus demand on a daily basis. This makes a hybrid Wind/PV solution an attractive option.

1.2. Previous works on RES in trolleybus grids

The major hurdle for the integration of RES in transportation grids is the intermittent nature of the vehicle scheduling. This leaves areas of the grid with low or no load for hour of the day when the RES is generating. In the case of PV, for example, an seasonal mismatch is

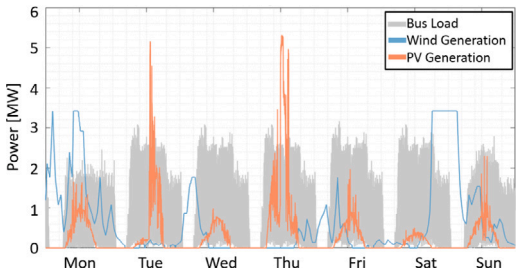

Fig. 5. Exemplary week number 9 of the per-second simulated bus demand, wind generation, and PV generation trends for the entire Arnhem grid. The PV and Wind systems are both sized to cover the whole grid demand for comparison reasons. The PV generation better follows the bus demand trend on a daily basis.

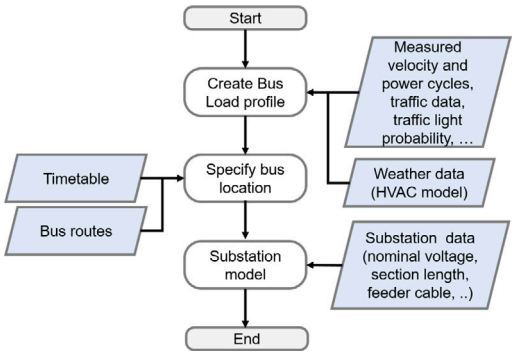

Fig. 6. The trolleygrid model flowchart.

very pronounced as well between the dense schedules and high heating demand of the winter months (with low PV generation) and the reduced scheduling and low cooling demands of the summer months (with high PV generation).

While some works exist in the field of PV in train, metro, and tram networks (e.g., Arévalo et al. (2021, 2020), Di Noia and Rizzo (2019), Cano et al. (2021), Capasso et al. (2015), Weiying et al. (2017), Al-Janahi et al. (2020), Şengör et al. (2017)), these rail systems are different than trolleygrids in terms of higher power levels, higher line voltages, more segmented electrical infrastructure, and less stochastic traffic conditions. This motivates the separate study of RES integration into trolleygrids. As mentioned earlier, the trolleygrid substations are unidirectional because of their rectifiers. This creates a major hurdle for the implementation of PV without storage on the DC side, as all the PV energy that is not consumed by the buses or the line losses (excess) should be curtailed. One possible solution is to place the PV on the AC side of the substation to allow a path for the PV system to use the LVAC as a storage (Fig. 1). The PV power is first inverted to AC (either single stage, or DC/DC and then DC/AC stages), allowing any excess energy to return to the AC grid and any trolleygrid power demand to be rectified again and sent to the trolleybuses (see Fig. 1). This is a first approach to placement on the AC side.

Another possibility is to connect the PV after its first DC stage to the trolleygrid. This, however, requires a separate study on the optimal feeding point location with respect to transmission losses and overhead line voltage drops, unless the PV is placed at the substation bus-bar as in some literature works (Bartłomiejczyk, 2018a). Nevertheless, this placement choice could only indirectly reduce the losses in the grid by increasing the feed-in voltage and would impose a lot of curtailment on the PV system, increasing thereby its utilization. Another approach in literature places the PV systems on all the substations based on the maximum allowable line impedance that is derived from the voltage drop limitations of the grid (Wazifehdust et al., 2019). This method is therefore more concerned with reducing line losses rather than increasing the sustainability of the grid and the utilization of the PV system. Furthermore, the PV model consists of an ideal curve multiplied by a randomized cloud factor, neglecting the modelling of environmental variations in the PV output power.

To the best knowledge of the authors, the only work that proposes a different PV size for trolleygrids substations based on their energy demand is (Bartłomiejczyk, 2018a). However, this work only suggests and estimated PV system size. Namely, that paper suggests placing 400–500 kW at large traction substations and 100–150 kW at small traffic ones. In comparison, the work presented here in this paper offers a systematic and specific sizing and placement approach as a function of the substation yearly energy demand.

Finally, trolleygrid networks have only been studied in tandem with PV systems. This paper offers the first Wind approach to trolleygrids.

In conclusion, for this paper, all RES placement would be done on the AC side, using detailed and verified RES and trolleygrid models. The systems will be studied both as decentralized (local, scaled for each substation demand) to allow for a more distributed instalment with lower space requirements and lower transmission losses, and as centralized (aggregated, scaled for the whole grid demand) as a way of benefiting from a less intermittent base load. Different and specific sizing, storage, and placement conclusions are drawn based on the size of the yearly demand of different substations of the trolleygrid, allowing for better RES system performance.

1.3. Paper contributions

The research has the following contributions:

1. The first sizing and placement study of wind and wind/PV hybrid systems as a renewable energy source for a trolleygrid system, both with and without storage, using detailed and verified trolleybus, trolleygrid, PV, and wind models
2. Six RES sizing and placement approaches that can cater for any trolleygrid substations by distinguishing them based on their demand size, presence of storage systems, and allowable exchange with the LVAC grid, using detailed and verified trolleybus, trolleygrid, PV, and wind models
3. A simple, original expression to find the performance limits of the PV system at a trolleygrid substation: the maximum achievable direct utilization and the highest direct load coverage (without storage systems)
4. A new decision factor (the PV traffic-view-factor) that assesses quickly which trolleygrid substations should have PV systems and which should not

1.4. Paper structure

This paper started by introducing the trolleybus system and the scope of this paper. Section 2 details the modelling methodology and the key definitions. The remaining Sections 3–8 report on six different sizing and placement options for RES in the trolleygrid: Decentralized energy-neutral PV without storage, decentralized PV of different sizes without storage, Decentralized PV sized for 50% utilization and without storage, Decentralized PV system of different sizes and with storage, decentralized PV system of different sizes and with storage and AC exchange limitations (PV curtailing), and centralized PV and/or Wind systems with/without storage. Finally, Section 9 offers conclusions and future work recommendations.

2. Methodology

2.1. Modelling the trolleybus grid

The trolleygrid model (Fig. 6) begins with the creation of bus demand from measured bus velocity and power cycles, and randomized traffic and stoplight probability data.

The bus powers are given by Eq. (1). While in traction mode, the bus power is simply the sum of the traction P_{tr} and the auxiliaries demand, P_{aux}. During braking, the bus power, P_{bus}, is the auxiliaries power P_{aux} plus the net exchanged with the grid P_{net}, and the excess energy P_{BR} that is wasted in the braking resistors. The auxiliaries consist of the P_{HVAC} that is a fraction (duty cycle) of the nominal HVAC power (36.5 kW), and P_{base} (taken here as 5 kW) that is the power of basic bus loads such as the doors, the screens, and the indoor lights, etc.

$$P_{bus,j} = \begin{cases} P_{net,j} + P_{aux,j} + P_{BR,j} & \text{if braking} \\ P_{tr,j} + P_{aux,j} & \text{if traction} \end{cases} \quad j = 1..N_{bus} \tag{1}$$

$$P_{aux} = P_{HVAC} + P_{base} \tag{2}$$

$$I_n = \begin{cases} P_n/V_{SN} & k = 1, \quad \& \quad n \neq SN \\ P_n/V_n & k \neq 1, \quad \& \quad n \neq SN \\ -\sum_{n \neq SN} I_n & n = SN \end{cases} \tag{3}$$

$$R_{n,n-1} = \rho \cdot |x_n - x_{n-1}| \tag{4}$$

$$V_n = \begin{cases} V_{n-1} - R_{n,n-1} \cdot I_{n,n-1} & n > SN \\ V_{n+1} - R_{n+1,n} \cdot I_{n+1,n} & n < SN \\ V_c & n = SN \end{cases} \tag{5}$$

$$V_c = \begin{cases} V_{SN} - R_f \cdot I_{SN} & i_{SN} > 0 \\ V_{SN} + V_{ds} & i_{SN} = 0 \end{cases} \tag{6}$$

The HVAC simulation model is based on a thermodynamic heat exchange model, its output is per-second power of the bus of the requirements to meet the inside cabin comfort conditions for the passengers. The HVAC model takes into account the conductive and convective heat transfer load (between the cabin and the external environment), the heat exchange due to the forced air ventilation and air circulation (air quality requirement), the air ventilation due to the opening of the doors for passenger transit (air exchange with the external environment), the direct, diffuse and reflected solar radiation heating of the bus external surfaces, and the metabolic heat gain from the passenger bodies.

Once the bus powers is known, the position of the bus loads under the trolleygrid is derived from the timetables and bus routes and the previously randomized traffic data.

The grid model calculates the bus voltages and, subsequently, the substation demand and losses and is based on the backward–forward sweep powerflow method (Wang et al., 2004). The model is explained in detail in Diab et al. (2022). The substation is modelled as a voltage-source slack node (SN), with a fixed nominal voltage, V_{SN}, at the rectifier output (i.e., before the feeder cable voltage drop) that delivers the total power demand on its supply zone (bus loads minus the regenerating bus exchanges).

Step 1: The model starts by reading and sorting the positions and powers of all the buses on the supply zone.

Step 2: As explained in Eq. (3), at the first iteration step, k, the current at each node, n, is the power of the node divided by V_{SN}, as an initial guess. At later iterations, with a voltage assigned to each node (from step 3 of the previous iteration), the current is obtained by dividing the power of each node by its voltage.

Step 3: The model sweeps across all nodes, starting from SN. The total impedance between two nodes n and n-1, $R_{n,n-1}$, is obtained from the equivalent impedance model (Eq. (4)) considering the impedance of the supply and return lines and the effect of the parallel connections between them. Each node voltage is the voltage of its adjacent node minus the resistive voltage drop between them (Eq. (5)). The voltage at the point of connection of the substation to the section, V_c, (see Fig. 1) is given by Eq. (6) where R_f is the resistance of the feeder cable, I_{SN} is the substation current, and V_{ds} is the voltage blocked by the substation rectifiers in case of overvoltages on the section (regenerative braking).

Step 4: The algorithm sweeps back across all the nodes and updates their currents. The slack node is then set to deliver the sum of all the node currents.

Step 5: As the model is concerned with non-reversible substations, I_{SN} in step 4 is checked if negative (oversharing of braking energy).

Step 5-Yes: If I_{SN} is negative, step 5-Yes reduces the power of the generating buses by the amount that is being sent into the substation. In practical terms, this means the buses are wasting this energy on their on-board braking resistors.

Step 6: If I_{SN} is not negative, the model checks for convergence and exits if it is achieved. A tolerance is defined for the current at each node (here, 0.2 A).

The model was verified using the trolleybus grid of Arnhem, the Netherlands. The error in the energy measurements stood at 3%.

2.2. Modelling the solar PV output

The PV model is a per-second simulation of the energy output of the solar panels. The model takes into accounts parameters such as: solar altitude (a_S), solar azimuth (A_S), global horizontal irradiance (GHI), diffuse horizontal irradiance (DHI), ambient temperature, ground temperature, and wind speed, to name a few. These values were obtained from Meteonorm (Koninklijk Nederlands Meteorologisch Instituut (KNMI), 2019). The shading from clouds is considered, however, enough distance is assumed between panels to allow for panel-on-panel shading to be neglected.

The optimal azimuth angle and the tilt angle of the PV module are identified through an iteration, in which the yearly irradiance per square meter on the module is calculated for each possible combination of azimuth and tilt. At these positions, the global irradiance on the model, G_M, is:

$$G_M = G_{M,dir} + G_{M,diff} + G_{M,refl} \tag{7}$$

Where the terms on the right hand side are the direct, diffuse, and reflected irradiance on the tilted module, respectively. The detailed equations for these terms are described in Smets et al. (2016). The PV module efficiency is a function of the module's temperature. This temperature is estimated as a function of meteorological parameters using a fluid dynamic model (energy balance between the PV module and the external surroundings). The model presented is based on Ref. Smets et al. (2016). Two main assumptions are steady state conditions, and that the whole PV module is at a single temperature. The second assumption is justified since the thickness of the solar cells (item of interest) is much smaller than that of the module and so is its heat capacity. The module's temperature, T_M, can be described as:

$$T_M = \frac{(1-R)(1-\eta)G_M + h_c T_a + h_{r,sky} T_{sky} + h_{r,gr} T_{gr}}{h_c + h_{r,sky} + h_{r,gr}} \tag{8}$$

Where R is the module reflectivity, η is the module's efficiency, h_c is the overall convective heat transfer coefficient (considering both top and back of the module), and T_a, T_{sky}, and T_{gr}, are the ambient, sky, and ground temperature, respectively. Finally, $h_{r,sky}$ and $h_{r,gr}$ are the linearized radiation heat transfer coefficient between the module and the sky and between the module and the ground, respectively. The linearization of $h_{r,sky}$ and $h_{r,gr}$ has the value of T_M in its expression, and hence Eq. (8) is solved iteratively.

The PV module's data sheet provided by the manufacturer show the effect on the efficiency by the deviation of the solar cell temperature from 25 °C (Standard Testing Conditions (STC)). The power at the maximum power point of the module, P_{MPP}, at T_M and STC irradiance G_{STC} can be calculated as:

$$P_{MPP}(T_M, G_{STC}) = P_{MPP} + \frac{\partial P_{MPP}}{\partial T}(STC)(T_M - T_{STC}) \tag{9}$$

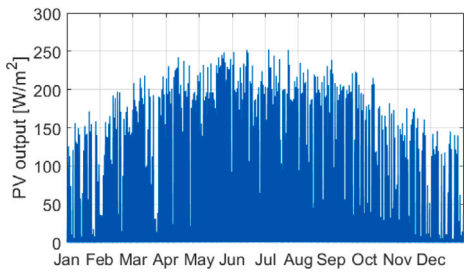

Fig. 7. Output of the yearly simulated PV generation in Arnhem in W/m2.

Table 1
Parameters for the wind model (Jonkman et al., 2009).

Hub height	90 m
Rotor radius, r	53 m
Cut-in wind speed, $v_{\text{cut-in}}$	3 m/s
Cut-out wind speed, $v_{\text{cut-out}}$	25 m/s
Rated wind speed, v_{rated}	11.4 m/s
Rated output power, P_{rated}	3.5 MW

with $\frac{\partial P_{\text{MPP}}}{\partial T}(\text{STC})$ as the power temperature coefficient from data sheets. From this, the efficiency at any irradiance and temperature can be calculated as:

$$\eta\left(T_{\text{M}}, G_{\text{STC}}\right) = \frac{P_{\text{mpp}}\left(T_{\text{M}}, G_{\text{STC}}\right)}{G_{\text{STC}} A_{\text{M}}} \tag{10}$$

where A_M is the module area. Rearranging Eq. (10), the efficiency temperature coefficient $\frac{\partial \eta}{\partial T}(\text{STC})$ can be obtained:

$$\eta\left(T_{\text{M}}, G_{\text{STC}}\right) = \eta(\text{STC}) + \frac{\partial \eta}{\partial T}(\text{STC})\left(T_{\text{M}} - 25°\text{C}\right) \tag{11}$$

Quantifying the effect of irradiance variation on solar cell performance is less straightforward than for the effect of temperature for lack of data from manufacturers. According to Smets et al. (2016), the overall module efficiency can be approximated as:

$$\eta\left(T_{\text{M}}, G_{\text{M}}\right) = \eta\left(25°\text{C}, G_{\text{M}}\right)\left[1 + \kappa\left(T_{\text{M}} - 25°\text{C}\right)\right] \tag{12}$$

where the first term represents the effect of irradiance and the second that of temperature, with κ computed as:

$$\kappa = \frac{1}{\eta(\text{STC})}\frac{\partial \eta}{\partial T} \tag{13}$$

representing the temperature effect on the performance relatively to the STC conditions efficiency. The selected module is the 'AstroSemi 365W' mono-crystalline panels from Astroenergy. The solar modules have a 365 Wp rated power and a 19.7% efficiency. The output of the model is seen in Fig. 7.

2.3. Modelling the wind turbine

The wind turbine model uses the same weather data as the PV model, and assumes that the turbine will be placed onshore (near Arnhem). The selected turbine is a 3.5MW turbine from NREL, based on their 5MW model, and the key parameters are presented in Table 1. The wind speed data is only available at 10 metres above ground level. The scaling to hub-height is done in two steps. First, from 10 to 60 metres to account for the surface roughness in the atmospheric boundary layer using the semi-empirical *log wind profile* fit described in Eq. (14). Second, from 60 m to the hub height of 90 m using the *power profile* expression represented in Eq. (15)(Oke, 2002).

$$u(z_2) = u(z_1)\frac{\ln((z_2 - d)/z_0)}{\ln((z_1 - d)/z_0)} \tag{14}$$

$$u(z_3) = u(z_2)\left(\frac{z_3}{z_2}\right)^{\alpha} \tag{15}$$

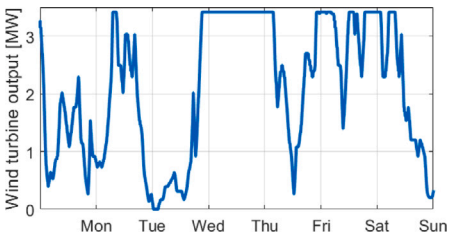

Fig. 8. Power output of the simulated wind turbine in Arnhem for one example week in February.

Here z_1, z_2 and z_3 are the heights at which the wind speeds u_1, u_2 and u_3 are measured or calculated i.e. at 10, 60, and 90 m, respectively. z_0 is the surface roughness factor (0.3 m for wind turbines on land), and α is the power factor which depends on the atmospheric conditions. It is common practice to assume that the atmosphere has on average a neutral stability (α=1) (Oke, 2002).

Once the wind velocity at hub height is known, the power delivered by the wind turbine is given by:

$$P_{\text{w}} = \begin{cases} \frac{1}{2}\rho_{\text{air}}\pi r^2 v_{\text{w}}^3 c_{\text{p}} & , v_{\text{cut-in}} < v_{\text{w}} < v_{\text{rated}} \\ P_{\text{rated}} & , v_{\text{rated}} \le v_{\text{w}} < v_{\text{cut-out}} \\ 0 & , \text{otherwise} \end{cases} \tag{16}$$

$$c_{\text{p}} = \frac{P_{\text{rated}}}{\frac{1}{2}\rho_{\text{air}}\pi r^2 v_{\text{rated}}^3} = 0.45 \tag{17}$$

Where ρ_{air} is the air density. An example of the power output of the turbine for one week is shown in Fig. 8.

2.4. Definition of system performance variables

The indicators defined and used to analyse the variation of the potential of integrating a PV system in a specific substation are:

PV Utilization, U_{PV}: This factor represents the independence from the LVAC grid as the percentage of solar power which is directly used to cover the load of the trolleygrid without being exchanged with the LVAC (Modes 1 and 3 in Fig. 3):

$$U_{\text{PV}} \triangleq \frac{\int_{\text{year}}(P_{\text{load}} - P_{\text{grid}})\,\text{d}t}{\int_{\text{year}} P_{\text{PV}}\,\text{d}t} \tag{18}$$

with P_{load} the total load power demand of the trolleybuses, P_{grid} the power delivered from the AC grid, and P_{PV} the PV generated power.

Direct Load Coverage, Λ: This factor is the fraction of the load that can be directly supplied by the output of the PV system, and it can be calculated by

$$\Lambda \triangleq \frac{\int_{\text{year}}(P_{\text{load}} - P_{\text{grid}})\,\text{d}t}{\int_{\text{year}} P_{\text{load}}\,\text{d}t} \tag{19}$$

It is possible to combine Eq. (18) and (19) as

$$\Lambda = \zeta \cdot U_{\text{PV}} \quad \text{(ignoring all converter losses)} \tag{20}$$

By defining the **Energy-Neutrality Ratio**, ζ, as:

$$\zeta \triangleq \frac{\int_{\text{year}} P_{\text{PV}}\,\text{d}t}{\int_{\text{year}} P_{\text{load}}\,\text{d}t} \tag{21}$$

Which becomes a normalized indication of the size of the PV system installed at a particular substation. For example, a PV system sized to yield the entire bus load demand in a year is said to have $\zeta = 1$.

However, accounting for the converter losses (see variables definition in Fig. 1), the energy delivered to the buses is found by:

Table 2
The characteristics of the Arnhem trolleygrid.

Number of Bus Lines	6
Number of buses	42
Number of sections	43
Number of Substations	18
Average section length [km]	1.1
Average daily sunshine duration [h]	4.0
Average yearly irradiance [kWh/m^2]	1165
Average trolleybus energy demand [kWh/km]	2.5
Peak trolleybus power demand [kW]	300
Average trolleybus power demand [kW]	70

Table 3
Summary of the characteristics of the six placement and sizing scenarios.

Sc.	RES type	RES placement	ζ	Storage	LVAC exchange
1	PV	Decentralized	1.0	No	Allowed
2	PV	Decentralized	Varying	No	Allowed
3	PV	Decentralized	Varying	No	Allowed
4	PV	Decentralized	Varying	Yes	Allowed
5	PV	Decentralized	Varying	Yes	Limited
6	PV/Wind	Centralized	1.0	Yes	N/A

$$\begin{aligned}\text{PV generation} &= \text{PV energy directly used} \\ &+ \text{PV energy sent} \\ &\text{to the AC grid and re-used later}\end{aligned} \tag{22}$$

$$\rightarrow \zeta \cdot \int_{\text{year}} P_{\text{load}}\,\mathrm{d}t = U_{\text{PV}} \cdot \int_{\text{year}} P_{\text{PV}}\,\mathrm{d}t \cdot \eta_{\text{DC}} \cdot \eta_{\text{AC}} \cdot \eta_{\text{r}} + (1 - U_{\text{PV}}) \cdot \int_{\text{year}} P_{\text{PV}}\,\mathrm{d}t \cdot \eta_{\text{DC}} \cdot \eta_{\text{AC}} \cdot {\eta_{\text{ts}}}^2 \cdot \eta_{\text{r}}$$

Re-arranging Eq. (22):

$$\int_{\text{year}} P_{\text{PV}}\,\mathrm{d}t = \frac{\zeta \cdot \int_{\text{year}} P_{\text{load}}\,\mathrm{d}t}{\eta_{\text{DC}} \cdot \eta_{\text{AC}} \cdot \eta_{\text{r}} \cdot (U_{\text{PV}} \cdot (1 - {\eta_{\text{ts}}}^2) + {\eta_{\text{ts}}}^2)} \tag{23}$$

Finally, combining Eq. (20) and (23):

$$\Lambda = \frac{\zeta}{\eta^*} \cdot U_{\text{PV}} \quad \text{(considering converter losses)} \tag{24}$$

Where η^* is the denominator term in Eq. (23). For the study in this paper, an efficiency of 99% is assumed for each conversion step (Fig. 1), and the trolleygrid weighted average of scenario I of 31% for U_{PV}. Ultimately:

$$\therefore \quad \eta^* \approx 0.957 \qquad \text{(this paper)} \tag{25}$$

2.5. Case study definition

2.5.1. The city of Arnhem

The case study chosen for this paper is the city of Arnhem, located in the eastern part of the Netherlands. The characteristics of its trolleygrid are presented in Table 2. The 6 studied scenarios are summarized in Table 3.

2.5.2. The power flow management

For all the studied scenarios, the aim is to send the PV power to the buses to increase the sustainability of the grid in the most efficient manner. This is mode 1 of Fig. 3. In the scenarios with storage, any excess PV energy is sent to the storage first (mode 2) and any further power is sent to the AC grid (mode 3). In the scenarios where the AC grid has limits on the AC power it can receive, such as in scenario V, the remaining PV energy is curtailed (mode 4).

Table 4
Size of the PV system in KW peak (kWp) at each substation for an energy neutral approach without storage (ζ = 1).

Substation	Size (kWp)	Substation	Size (kWp)
A	152	J	195
B	372	K	192
C	761	L	376
D	789	M	244
E	188	N	305
F	213	O	231
G	188	P	158
H	142	Q	73
I	238	R	276
		Total	**5093**
		Average	283

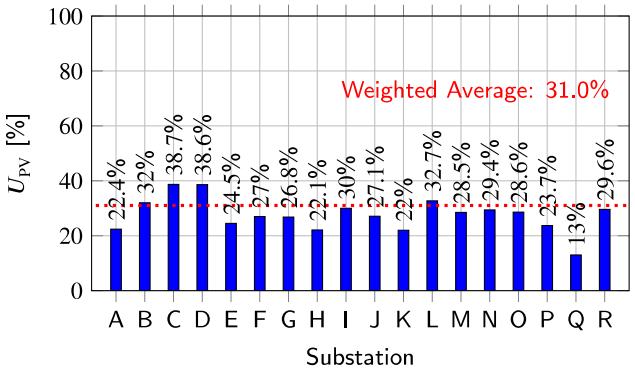

Fig. 9. PV Utilization (U_{PV}) at each substation in Arnhem for scenario 1: the decentralized energy-neutral approach without storage.

3. Scenario I: The decentralized energy-neutral approach without storage (ζ = 1)

The first approach is to place the PV in a decentralized manner (at each Substation (SS)), with a size that covers the yearly demand of the substation (energy neutral) and using the AC grid as a storage. The sizing results for the different substations in KW peak (kWp) are presented in Table 4, and U_{PV} is shown in Fig. 9.

The values of U_{PV} go between 13% and 38.7%, with a weighted average for the grid at 31.0%. This means that 69.0% of the PV power is sent into the AC grid to be used at a later stage. More specifically, power is sent to the grid in the summer to be recalled in the winter. On the other hand, only 32.4% of the load is covered (Eq. (24)). In this manner, the AC grid is still practically providing the trolleygrid load during the largest part of the year.

The results are unsatisfactory because the resulting PV system is too large for the urban environment (over 5 MWp) for only a 32.4% direct load coverage, and a significant dependency on the AC grid. It is not therefore not advisable to size the PV in a fully decentralized, energy-neutral manner without storage.

4. Scenario II: Varying the PV system size without storage

The decentralized energy-neutral approach without storage results were not satisfactory because the low PV utilization meant a strong dependence on the grid. This section looks at the varying the PV size from ζ = 0.1 to 2.0 as another method for avoiding using storage. The motivation is that undersized PV systems (ζ < 1) are interesting because they have a high U_{PV} since they do not generate a lot and therefore do not need to dump a lot. Consequently however, they do not offer a lot of direct load coverage. On the other hand, oversized PV systems (ζ>1) would offer a high direct load coverage and their excessive energy can

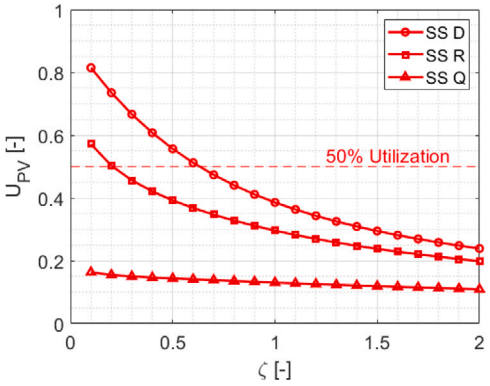

Fig. 10. PV Utilization, U_{PV}, for three substations in Arnhem: Largest (SS-D), average (SS-R), and smallest (SS-Q).

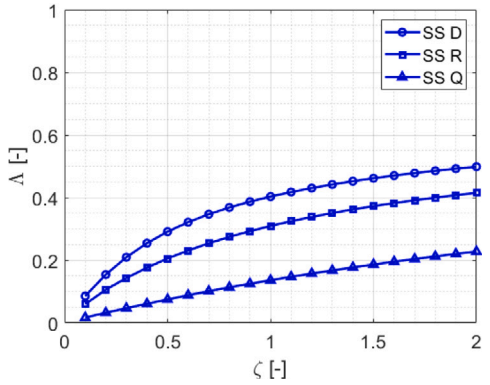

Fig. 11. Direct load coverage, Λ, for three substations in Arnhem: Largest (SS-D), average (SS-R), and smallest (SS-Q).

be curtailed. The motive is that this procedure is cheaper than installing storage systems as these systems cost more than the PV systems.

Figs. 10 and 11 show the results of three substations in Arnhem: The highest (SS-D), average (SS-R), and lowest (SS-Q) substation demand size. Over-sizing the system does not seem to produce interesting direct load coverage results. By doubling the PV system size from $\zeta = 1$ to $\zeta = 2$, the direct load coverage increases only by 10 percentage points (40% to 50%), 12 points (30% to 42%), and 9 points (14% to 23%) for SS-D, SS-R, and SS-Q, respectively.

On the other hand, under-sizing the PV system to increase its utilization rapidly decrease its direct load coverage. While the U_{PV} can go beyond 80% for SS-D, for example, the direct load coverage, Λ, at that system size is merely 9%.

Undersizing PV systems, without storage, at small substations does not produce promising results. On the other hand, there is a potential for small PV systems at large substations, even if the absence of storage limits them to system sizes that would not offer a lot of load coverage.

5. Scenario III: Marginal utilization sizing approach (U_{PV}=50%) without storage

5.1. Sizing the PV system

It was concluded that the PV Utilization drops rapidly for large systems with increasing system size. Another approach is to size using the marginal utilization, i.e. the difference in utilization brought on by an increment in the system size. In this method, the system size is increased until the point where adding 1 kWp of PV would result in more of its yearly yield $E_{y/kWp}$ being dumped than utilized. In Arnhem,

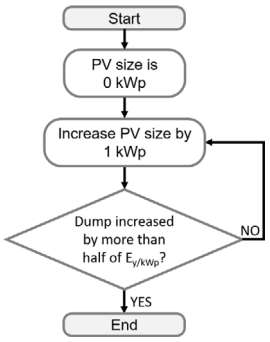

Fig. 12. Flowchart for the PV system sizing in the Marginal Utilization Sizing approach (U_{PV} = 50%) without storage (scenario III).

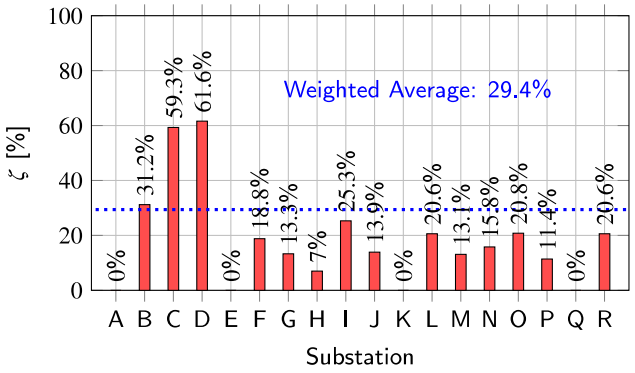

Fig. 13. Attainable fraction of energy neutral sizing for each substation using the Marginal Utilization sizing approach. For substations A, E, K, and Q, no PV is advised.

this value is 1155.7 kWh/kWp. In simpler terms, this is equivalent to sizing the system at each substation for U_{PV}=50%.

The method is explained by the flowchart in Fig. 12, and the results are presented in Fig. 13.

For 4 out of the 18 substations in Arnhem, namely substations A, E, K, and Q, the suggested PV system size is zero. This is already expected from Fig. 10 as SS-Q does not reach the 50% utilization line even for very small PV system sizes. Fig. 13 also echoes the results found for SS-D and SS-R in Fig. 10 looking at the system sizes at the 50% utilization line.

5.2. Traffic view factor

The wide difference between the suggested PV system sizing for the substations in Fig. 13 can be traced again back to Fig. 2. The bus traffic under some substations is so infrequent that the PV system would not *see* a bus for long periods of time. To further explain this difference, define the parameter "bus traffic view factor of the PV" for a substation as the fraction of the PV generation time where the PV system sees *at least* one bus under the substation. Mathematically, it can be expressed as:

$$\Phi_{B/PV} \triangleq \frac{\Sigma \text{time}(PV \cap Bus)}{\Sigma \text{time}(PV)} \tag{26}$$

The $\Phi_{B/PV}$ in Arnhem varies between 0.17 and 0.89, with an average of 0.62. This means that, on average, a PV system in Arnhem does not see a bus for 38% of the sunshine hours. It follows then that even an infinitely small PV system is not able to power the buses without storing a considerable part of its energy in the AC grid. In mathematical terms:

$$\lim_{PV\ Size \to 0} U_{PV} = \Phi_{B/PV} \tag{27}$$

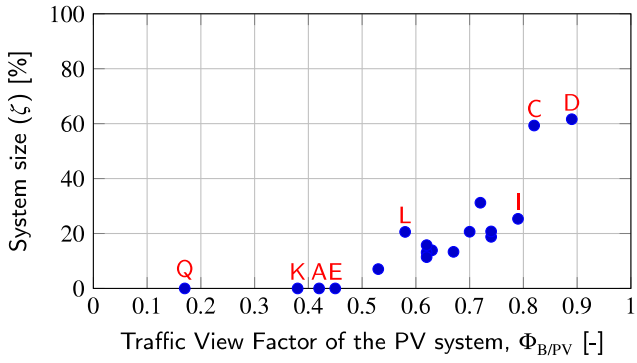

Fig. 14. PV system size as a fraction of the Energy Neutral size for each substation versus the traffic view factor of the PV system $\Phi_{B/PV}$.

As for the direct load coverage, Λ, the maximum attainable value, even for an infinitely large system, would be the fraction of the trolleybus demand that occurs during the sun hours. With no storage system in place, the PV system cannot power the bus traffic before sunrise and after sunset. Assuming an average consumption by the buses throughout the year, the ratio of energy consumption can be approximated by the ratio of time duration as expressed by:

$$\lim_{\text{PV Size}\to\infty} \Lambda = \frac{\Sigma^{\text{time(PV}\cap\text{Bus)}} P_{\text{Bus}}}{\Sigma^{\text{year}} P_{\text{Bus}}} \approx \frac{\Sigma\text{time(PV} \cap \text{Bus)}}{\Sigma\text{time(Bus)}} \tag{28}$$

The estimate offered by Eq. (28) can be made even more accurate by averaging the limit for each month of the year rather than for the whole year. This is because in the winter months, the sun hours are shorter and the bus load is higher, while in the summer months, the opposite is true. Fig. 14 shows a trend between the traffic view factor of the PV system and the system size for 50% PV Utilization. The four substations A, E, K, and Q that have a suggested PV size of 0 kWp by this method can be traced to having a $\Phi_{B/PV} < 50\%$. This means that the PV system at these locations does not see the bus for more than half of the sun hours, consequently, no PV system size will reach a $U_{PV} > 50\%$.

An increasing trend is reported in the same figure between $\Phi_{B/PV}$ and the system size for 50% PV Utilization. This motivates the placement of PV systems at high $\Phi_{B/PV}$ locations. However, some trends are not fully explained by only looking at this parameter alone. For example, substations I and L have about the same system size recommendation (25.3% and 20.6%, respectively) despite SS-I seeing about 20 percentage points higher in traffic than SS-L. Additionally, SS-I and SS-C have about the same $\Phi_{B/PV}$, yet the recommendation for SS-C is a system size of about 2.5 times that of SS-I ($\zeta = 59.3\%$). One explanation of this behaviour is that the $\Phi_{B/PV}$ only takes into account the presence of a load, not its magnitude. SS-C has, in fact, 3.2 times the load demand of SS-I. Fig. 10 already predicted that larger substations see a better PV Utilization.

The Marginal Utilization Approach offers a $\zeta = 29.4\%$ as a weighted grid average, which translates to only a 15.4% direct load coverage, Λ, according to Eq. (24). This method is superior then in performance if compared to the first scenario of the decentralized energy-neutral approach. In the earlier method, an energy neutral system ($\zeta = 100\%$) offered 31% direct load coverage, while this method offers half of this direct load coverage ($\Lambda = 15.4\%$) by installing less than a third of the former system size ($\zeta = 29.4\%$), meaning far less exchange with the grid and a much lower cost per kWp installed. However, the disadvantage of the marginal utility method, is that it leaves out some substations completely to be powered by the grid (here, SS-A, E, K, and Q).

6. Scenario IV: The decentralized generation with storage approach

This method looks at storage as a way to increase the utilization of the PV system and its load coverage. Figs. 15 and 16 summarize the results of the direct load coverage, Λ, for different PV system sizes, ζ, and storage sizes for substations D and Q, respectively.

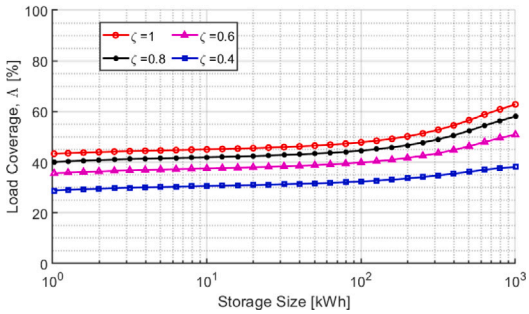

Fig. 15. Direct load coverage, Λ, for different ζ values and storage sizes for the large substation D.

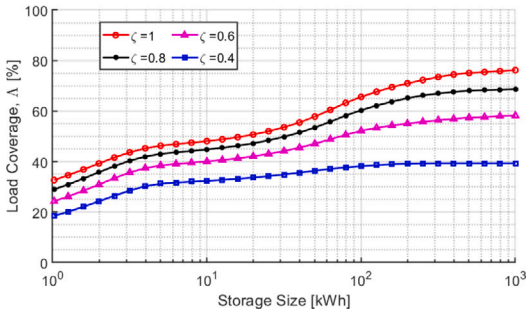

Fig. 16. Direct load coverage, Λ, for different ζ values and storage sizes for the small substation Q.

Storage does not seem to benefit the direct load coverage for a large substation such as SS-D, until a steep increase in direct load coverage at the order of hundreds of kWh. This is because high load/traffic substations already have the advantage of a steady load base (see Fig. 2) that directly utilizes more of the daily PV generation. An advantage is only observed when stepping into systems at the order of seasonal storage, where these large storage systems can gather the PV energy in the summer to be used in the winter. However, a storage system as large as 1 MWh, has only increased the direct load coverage of SS-D from 44% to 63% for the $\zeta = 1$ case.

Meanwhile, for a small substation such as SS-Q, storage benefits the direct load coverage through a steep increase in the direct load coverage even for relatively small storage system sizes. This can again be traced back to Fig. 2, where it is clear that a mismatch is far more pronounced between the PV and the load in low traffic substations. Small storage systems can help carry the PV energy generated in the short no-load periods between buses on the trolleygrid section. Storage systems of the order of seconds/minutes ($<10^1$kWh) affect all the ζ cases by 12 to 17 percentage points higher in direct load coverage. Storage on the daily level (between 10^1 and 10^2 kWh) has also benefited the direct load coverage. However, while the increase is still steep in the cases of $\zeta = 0.8$ or 1.0, with another 16 percentage points, it is less pronounced in the cases of $\zeta = 0.6$ and 0.4, where the direct load coverage increased only by 12 and 5 percentage points, respectively. This is because at large PV system sizes (high generation), the mismatch in generation versus load becomes more important than the temporal mismatch between the presence of a load and the PV generation (more important role at low generation levels). In simpler terms, there is more to store with larger PV systems on a daily level, while smaller systems start to behave sooner on the storage scale like a seasonal-storage scenario because their small daily generation is already stored completely by any system between 10^1 and 10^2 kWh. In conclusion, for large substations, storage is not recommended and smaller PV systems

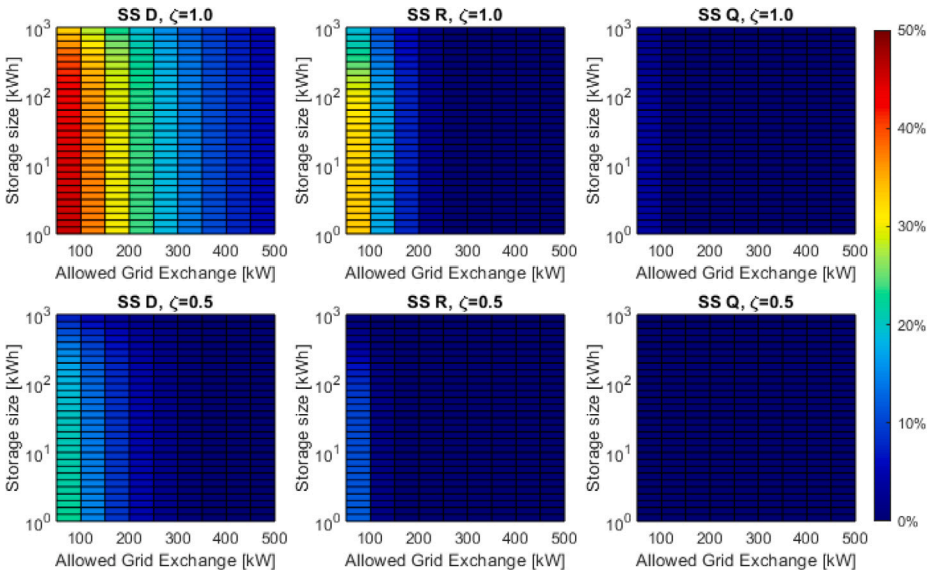

Fig. 17. Percentage of curtailed PV energy as a function of the storage system size and the allowed exchange with the AC grid for different PV system sizes at substations D (trolleygrid highest load demand), R (average demand), and Q (lowest demand).

seem more attractive. Meanwhile, a larger PV system size (high ζ) and a storage system are recommended for smaller substations.

7. Scenario v: The LVAC grid exchange limit approach (PV curtailment)

So far, the sizing strategies have taken the grid as a fully-available sink to the PV excess energy without considering power quality issues or local policy restrictions. The sizing of the PV and storage systems in this section considers the maximum allowable exchange with the AC grid, and curtails (wastes) the remaining PV generation (Mode 4 of Fig. 3). Fig. 17 shows the percentage of the PV generation that is curtailed at $\zeta = 1$ and 0.5 and various storage sizes and allowable power exchange levels with the AC grid, for substations D, R and Q, respectively.

The busy substation D needs a large PV system and is therefore more prone to sending higher surges of power, and more frequently, to the AC grid. The curtailment can be as high as 45.5% and 22.7% for $\zeta = 1$ and $\zeta = 0.5$, respectively. For the average substation R, the values can be as high as 33.1% and 12.1%, for $\zeta = 1$ and $\zeta = 0.5$.

The smaller substation Q, on the other hand, requires a small PV system. For a size of only $\zeta = 0.5$, the PV output can be used entirely (maximum curtailment of 0.0%). For $\zeta = 1$, the curtailment is only 3.9% in the most restrictive cases, but is 0.0% if an exchange of 100 kW is permitted.

Small substations, therefore, offer a more feasible implementation of PV system with minimal storage and grid interference. Interesting to note that the curtailment value is not affected much by the storage size when strict dumping levels are imposed. This is again a consequence of the seasonal variation of PV and the bus load and the necessity for seasonal storage, and imposes a hurdle on the implementation of PV systems for the trolleygrid energy-neutrality. The same trend is observed for the larger substations, where the curtailment is considerable. This reconfirms the suggestion of the scenario IV that small substations should have large PV systems and vice-versa.

8. Scenario VI: The centralized energy-neutral wind and PV approach (aggregated approach)

The final approach is to size the PV system or the Wind system in an aggregated manner for the whole grid. This can be done by contracting a PV or Wind energy supplier, for example, the way the

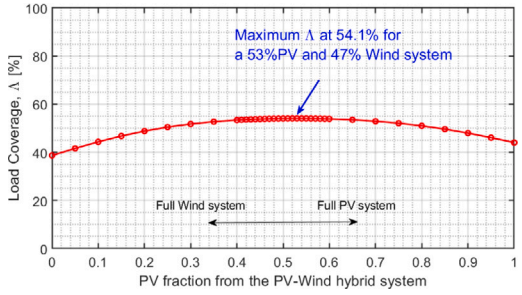

Fig. 18. Direct Load coverage as a function of the RES system composition (PV and Wind) without storage.

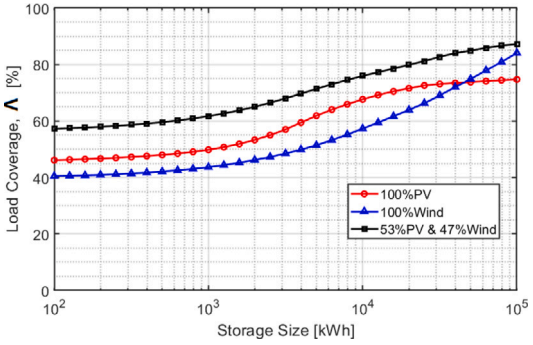

Fig. 19. Direct Load coverage as a function of the hybrid RES system composition (PV and Wind) with storage.

Dutch railways operate. The advantage of this method from the point of view of utilization is that on the grid-level there are loads present at all times, unlike at the fragmented substation-level.

Fig. 18 shows the direct load coverage, Λ, of the aggregated approach from a full wind system to a full PV system. The full wind system achieves a Λ of 39% while the full PV system reaches 45%. The highest Λ value of 54.1% is obtained for a hybrid system of 53% PV and 47% wind. The superior outcome of the hybrid approach is an expected result as it has been explained earlier in Figs. 4 and 5 that while the PV generation matches the bus profile better on a daily basis, the wind

generation matches it better on a yearly basis. A hybrid solution would therefore have a lower need for storage systems.

Fig. 19 shows the increase in direct load coverage by including storage. The aggregated grid behaves like a large substation, which explains why the PV system equipped with storage does not see much of an increase in load coverage, as seen earlier in Fig. 15 when studying a single, high-traffic substation. However, the wind system equipped with storage overtakes the PV system and becomes almost equal in performance to the hybrid system from storage systems at the order of daily storage (10^4 kWh at this system size). This is because the wind system benefits more from the daily storage systems, while the PV needs storage systems at the seasonal level to finally start yielding advantages.

9. Conclusions

This paper looked into a nuanced approach to the placement and sizing of RES systems at different trolleygrid substations based on the expected bus power demand. Six different approaches (Section 3 to 8) were simulated and assessed based on the direct RES utilization and the direct load coverage of their suggested RES systems.

In conclusion, the best recommendation for the sustainable powering of the trolleygrid from the AC side is to aggregate the generation for the whole grid rather than place decentralized RES systems. A hybrid PV/Wind system proved to be superior to a full wind or full PV option. In case a decentralized system is still preferred for sizing or location limitations, the recommendation is to undersize the PV systems for large substations (aiming for U_{PV}=50%) and without storage, while the smaller substations could be sized for full energy neutrality and would benefit greatly from storage systems, even at relatively small sizes.

However, as Fig. 14 exposed, more work is recommended on further Key Performance Indicators (KPIs) for a nuanced approach to substations beyond their load size alone, since it is clear that other variables affect the PV Utilization as well, and warrant our attention. Furthermore, more research is encouraged into the integration of more loads into the trolleygrid (EV chargers, for example), to create a more constant base load for the PV system, both increasing its utilization by the same advantages of the aggregated scenario, and sharing the cost of sustainable energy production among multiple public services.

Finally, the critical recommendation of sizing the PV system at large substations for U_{PV}=50% calls for a simple estimation approach of the expected utilization of a PV system at any trolleygrid substation without the need for extensive grid and RES modelling.

CRediT authorship contribution statement

Ibrahim Diab: Conceptualization, Methodology, Software, Validation, Investigation, Data curation, Writing – original draft. **Bram Scheurwater:** Software, Validation, Investigation, Data curation, Writing – original draft. **Alice Saffirio:** Software, Validation, Investigation, Data curation, Writing – original draft. **Gautham Ram Chandra-Mouli:** Funding acquisition, Project administration, Supervision, Writing – review & editing, Resources. **Pavol Bauer:** Funding acquisition, Project administration, Supervision, Writing – review & editing.

Declaration of competing interest

The authors declare that they have no known competing financial interests or personal relationships that could have appeared to influence the work reported in this paper.

Acknowledgments

This work has been funded under the Trolley2.0 project within Electric Mobility Europe. The authors would like to also thank Hans Aldenkamp and Niek Limburg from Connexxion, Arnhem, for their valuable input.

References

Al-Janahi, S.A., Ellabban, O., Al-Ghamdi, S.G., 2020. Technoeconomic feasibility study of grid-connected building-integrated photovoltaics system for clean electrification: A case study of Doha metro. Energy Rep. 6, 407–414.

Alliance, G.B., 2019. A vision for a sustainable battery value chain in 2030: Unlocking the full potential to power sustainable development and climate change mitigation. In: World Economic Forum. Geneva, Switzerland.

Arévalo, P., Cano, A., Benavides, J., Jurado, F., 2021. Feasibility study of a renewable system (PV/HKT/GB) for hybrid tramway based on fuel cell and super capacitor. IET Renew. Power Gener. 15 (3), 491–503.

Arévalo, P., Cano, A., Jurado, F., 2020. Comparative study of two new energy control systems based on PEMFC for a hybrid tramway in Ecuador. Int. J. Hydrogen Energy 45 (46), 25357–25377.

Bartłomiejczyk, M., 2017. Practical application of in motion charging: Trolleybuses service on bus lines. In: 2017 18th International Scientific Conference on Electric Power Engineerin. EPE, IEEE, pp. 1–6.

Bartłomiejczyk, M., 2018a. Potential application of solar energy systems for electrified urban transportation systems. Energies 11 (4), 954.

Bartłomiejczyk, M., 2018b. Smart grid technologies in electric power supply systems of public transport. Transport 33 (5), 1144–1154.

Borowik, L., Cywiński, A., 2016. Modernization of a trolleybus line system in Tychy as an example of eco-efficient initiative towards a sustainable transport system. J. Cleaner Prod. 117, 188–198.

Brunton, L., 1992. The trolleybus story. IEE Rev. 38 (2), 57–61.

Cano, A., Arévalo, P., Benavides, D., Jurado, F., 2021. Sustainable tramway, techno-economic analysis and environmental effects in an urban public transport. A comparative study. Sustain. Energy, Grids Netw. 26, 100462.

Capasso, A., Lamedica, R., Podestà, L., Ruvio, A., Sangiovanni, S., Lazaroiu, G., Maranzano, G., 2015. A measurement campaign in a metro trains deposit/maintenance and repair site for PV production optimal sizing. In: 2015 IEEE 15th International Conference on Environment and Electrical Engineering. EEEIC, IEEE, pp. 956–961.

Cornic, D., 2010. Efficient recovery of braking energy through a reversible DC substation. In: Electrical Systems for Aircraft, Railway and Ship Propulsion. IEEE, pp. 1–9.

Di Noia, L.P., Rizzo, R., 2019. Analysis of integration of PV power plant in railway power systems. In: 2019 8th International Conference on Modern Power Systems. MPS, IEEE, pp. 1–5.

Diab, I., Saffirio, A., Chandra Mouli, G.R., Tomar, A.S., Bauer, P., 2022. A complete DC trolleybus grid model with bilateral connections, feeder cables, and bus auxiliaries. IEEE Trans. Intell. Transp. Syst. 1–12. http://dx.doi.org/10.1109/TITS.2022.3157080.

Europea, C., 2013. Together towards competitive and resource-efficient urban mobility.

Fitzová, H., Matulová, M., 2020. Comparison of urban public transport systems in the Czech Republic and Slovakia: Factors underpinning efficiency. Res. Transp. Econ. 81, 100824.

Iannuzzi, D., Lauria, D., Tricoli, P., 2012. Optimal design of stationary supercapacitors storage devices for light electrical transportation systems. Opt. Eng. 13 (4), 689–704.

Jonkman, J., Butterfield, S., Musial, W., Scott, G., 2009. Definition of a 5-MW reference wind turbine for offshore system development. Technical Report, National Renewable Energy Lab.(NREL), Golden, CO (United States).

Kołoś, A., Taczanowski, J., 2016. The feasibility of introducing light rail systems in medium-sized towns in Central Europe. J. Transp. Geogr. 54, 400–413.

Koninklijk Nederlands Meteorologisch Instituut (KNMI), 2019. Meteonorm world solar irradiance data. URL https://meteonorm.com.

Kratz, S., Krueger, B., Wegener, R., Soter, S., 2018. Integration of photovoltaics into a smart trolley system based on SiC-Technology. In: 2018 IEEE 7th International Conference on Power and Energy. PECon, IEEE, pp. 168–173.

Kratz, S., Schmidt, A., Krueger, B., Wegener, R., Soter, S., 2019. Power supply of a short-range public transportation system based on photovoltaics-potential analysis and implementation. In: 2019 IEEE 46th Photovoltaic Specialists Conference. PVSC, IEEE, pp. 3077–3081.

Oke, T.R., 2002. Boundary Layer Climates. Routledge.

Rufer, A., Hotellier, D., Barrade, P., 2004. A supercapacitor-based energy storage substation for voltage compensation in weak transportation networks. IEEE Trans. Power Deliv. 19 (2), 629–636.

Salih, M., Baumeister, D., Wazifehdust, M., Steinbusch, P., Zdrallek, M., Deskovic, P., Küll, T., Troullier, C., 2018a. Impact assessment of integrating novel battery-trolleybuses, PV units and EV charging stations in a DC trolleybus network. In: 2nd E-Mobility Power System Integration Symposium. MOSI Symposium, pp. 1–6.

Salih, M., Baumeister, D., Wazifehdust, M., Steinbusch, P., Zdrallek, M., Mour, S., Deskovic, P., Küll, T., Troullier, C., 2018b. Optimized positioning for storage systems in an LVDC traction grid with non-receptive power sources and photovoltaic systems. unpublished.

Şengör, I., Kılıçkıran, H.C., Akdemir, H., Kekezoğlu, B., Erdinc, O., Catalao, J.P., 2017. Energy management of a smart railway station considering regenerative braking and stochastic behaviour of ESS and PV generation. IEEE Trans. Sustain. Energy 9 (3), 1041–1050.

Shekhar, A., Chandra Mouli, G.R., Bandyopadhyay, S., Bauer, P., 2021. Electric vehicle charging with multi-port converter based integration in DC trolley-bus network. In: 2021 IEEE 19th International Power Electronics and Motion Control Conference. PEMC, IEEE, pp. 250–255.

Smets, A.H., Jäger, K., Isabella, O., van Swaaij, R., Zeman, M., 2016. Solar Energy: The Physics and Engineering of Photovoltaic Conversion Technologies and Systems. UIT.

Tomar, A.S., Veenhuizen, B., Buning, L., Pyman, B., 2018. Estimation of the size of the battery for hybrid electric trolley busses using backward quasi-static modelling. In: Multidisciplinary Digital Publishing Institute Proceedings, Vol. 2, no. 23. p. 1499.

Wang, C., Cai, W., Lu, X., Chen, J., 2007. CO2 mitigation scenarios in China's road transport sector. Energy Convers. Manage. 48 (7), 2110–2118.

Wang, Z., Chen, F., Li, J., 2004. Implementing transformer nodal admittance matrices into backward/forward sweep-based power flow analysis for unbalanced radial distribution systems. IEEE Trans. Power Syst. 19 (4), 1831–1836.

Warin, Y., Lanselle, R., Thiounn, M., 2011. Active substation. In: World Congress on Railway Research. Lille, pp. 22–26.

Wazifehdust, M., Baumeister, D., Salih, M., Steinbusch, P., Zdrallek, M., Mour, S., Troullier, C., 2019. Potential analysis for the integration of renewables and EV charging stations within a novel LVDC smart-trolleybus grid.

Weiying, W., Mingliang, W., Qi, L., Weirong, C., 2017. Method for improving power quality of metro traction power supply system with PV integration. In: 2017 Chinese Automation Congress. CAC, IEEE, pp. 1682–1685.

Wołek, M., Wolański, M., Bartłomiejczyk, M., Wyszomirski, O., Grzelec, K., Hebel, K., 2021. Ensuring sustainable development of urban public transport: A case study of the trolleybus system in Gdynia and Sopot (Poland). J. Cleaner Prod. 279, 123807.

Wu, W., Lin, Y., Liu, R., Li, Y., Zhang, Y., Ma, C., 2020. Online EV charge scheduling based on time-of-use pricing and peak load minimization: Properties and efficient algorithms. IEEE Trans. Intell. Transp. Syst..

Zhang, D., Jiang, J., Zhang, W., et al., 2015. Robust and scalable management of power networks in dual-source trolleybus systems: A consensus control framework. IEEE Trans. Intell. Transp. Syst. 17 (4), 1029–1038.

Zhang, D., Jiang, J., Zhang, W., et al., 2017. Optimal power management in DC microgrids with applications to dual-source trolleybus systems. IEEE Trans. Intell. Transp. Syst. 19 (4), 1188–1197.